Proceedings Paper:
Drummond, R., Guiver, C., Turner, M.C. et al. (2025) Hotspots in lithium-ion battery pouch cells: models and bounds. In: 2025 IEEE Conference on Control Technology and Applications (CCTA). 2025 IEEE Conference on Control Technology and Applications (CCTA), 25-27 Aug 2025, San Diego, CA, USA. Institute of Electrical and Electronics Engineers (IEEE), pp. 396-401. ISBN: 9798331539092. ISSN: 2768-0762. EISSN: 2768-0770.

https://doi.org/10.1109/ccta53793.2025.11151280

Hotspots in lithium-ion battery pouch cells: Models and bounds

Ross Drummond, Chris Guiver, Matthew C. Turner, Eloise C. Tredenick, Stephen R. Duncan

***Abstract*— Lithium-ion batteries have grown larger in recent years in response to the need to increase pack-level energy densities. One of the main issues that emerges in these large format cells are heterogeneities. In particular, temperature hotspots in large pouch cells have been shown to influence degradation rates and fast charging limits. Motivated by these issues, this paper proposes computationally efficient models and bounds to characterise thermal hotspots in pouch cells. The models are validated against experimental data and shown to capture the spread in temperature across the pouch cell. The bounds exploit *external positivity* of the underlying system to improve scalability and are shown to be tight under constant current cycling. Through these results, bounds for the maximum temperature a pouch cell will experience during an arbitrary use-profile can be computed at scale and so be used to support battery safety and control.**

***Index Terms*— Lithium-ion batteries, externally positive systems, thermal hotspots.**

I. Introduction

Whilst the chemical compositions of commercial lithium-ion batteries have remained relatively unchanged over the past twenty years or so, with lithium iron phosphate $LiFePO_4$ (LFP), lithium nickel manganese cobalt oxide $Li[Ni_xMn_yCo_z]O_2$ (NMC), and lithium nickel cobalt aluminium oxide $Li[Ni_xCo_yAl_z]O_2$ (NCA) cathodes and graphite anodes dominating [1], their form factors have undergone major upgrades. One of the most successful techniques adopted by cell manufacturers to increase energy densities has been to simply make them larger. Specific examples of these larger cells (which are now being mass-produced) include the scale-up from 18650 to 21700 cylindrical cells [2] and the push towards large format pouch and prismatic cells [3] such as "*blade batteries*". This approach of simply making lithium-ion cells bigger has proven to be a relatively scalable way to deliver higher performance batteries in the meantime as we wait for the next generation of batteries, notably solid-state batteries, to reach technological and economic maturity [4]. The benefits of larger cells are predominately felt at the pack-level, through improved packing densities and a reduction in the relative fraction of superfluous material in the pack (e.g. from the wiring and casings). As recent studies such as [1] have shown, the impact of these superfluous materials can be significant; for example [1] estimated a cell-to-pack drop-off in energy density from ≈ 250 Wh kg^{-1} to ≈ 150 Wh kg^{-1} for a graphite-SiOx||NCA cell. Reducing this drop-off by designing more efficient packs, i.e. through more efficient packing with larger cells, could be as effective as more challenging solutions for increasing pack performance, such as discovering new electrode materials.

One of the main problems observed in large format lithium-ion batteries are *heterogeneities* in their state-of-charge, current, degradation, and temperature [3], [5]. In particular, the role of temperature heterogeneities, as observed through the formation of hotspots, has received recent attention [3], [6], [7]. The role of temperature on the electrochemical response of a battery is complex, with several recent studies highlighting its growing influence on our understanding of phenomena such as fast charging performance [5] and degradation rates [3]. Reducing these hotspots, or at least understanding how they form, could then improve battery performance and support the next generation of packs.

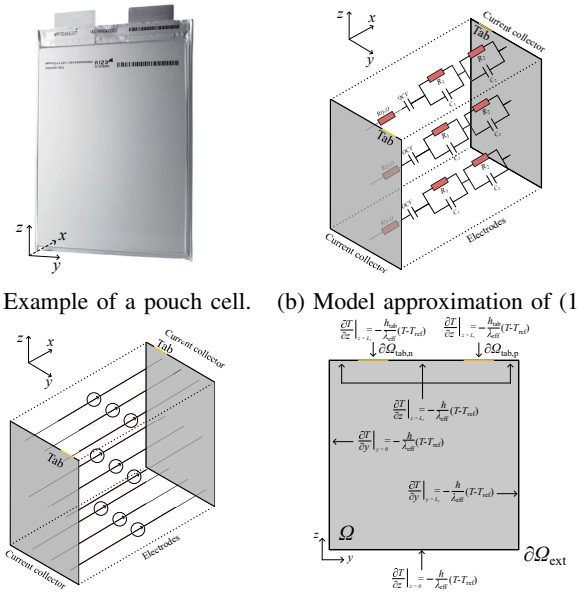

(a) Example of a pouch cell. (b) Model approximation of (1).

(c) Model approximation of (4). (d) 2D model domain

Fig. 1: Pouch cell model schematics of Eqns. (1) and (4).

Ross Drummond is with the School of Electrical and Electronic Engineering, University of Sheffield, UK. Email: ross.drummond@sheffield.ac.uk.

Chris Guiver is with the School of Computing, Engineering & the Built Environment, Edinburgh Napier University, Edinburgh, EH10 5DT, UK. Email: c.guiver@napier.ac.uk.

Matthew C. Turner is with the School of Electronics and Computer Science, University of Southampton, Southampton, SO17 1BJ, UK. Email: m.c.turner@soton.ac.uk.

Eloise C. Tredenick is with the Faculty of Science and Technology, University of Canberra, 2617, AUS. Email: eloise.Tredenick@canberra.edu.au.

Stephen R. Duncan is with the Department of Engineering Science, University of Oxford, Oxford OX1 3PJ, UK. Email: stephen.duncan@eng.ox.ac.uk.

Variable	Description	Unit
i_x	Current density through electrode thickness	A m^{-2}
I	Current density in the current collector	A m^{-2}
I_{app}	Applied current	A
R	Cell series resistance	Ω
SoC	Local state of charge	-
T	Temperature	K
t	Time	s
U	Open circuit voltage (OCV)	V
V	Voltage	V
v_1	Voltage across RC-pair	V
v_2	Voltage across RC-pair	V
x	Direction through cell	m
y	Direction along cell width	m
z	Direction along cell height	m

TABLE I: Variables of the pouch cell models.

A. Contribution

The aim of this paper is to develop a method to bound the temperature distribution in large format lithium-ion batteries. The main contributions are:

1) A control-orientated model for the temperature distribution across large format pouch cells is developed (Section II-C).
2) The model is validated against experimental data from [5] and compared against the more complex model from [8] (Section III).
3) Scalable bounds for the maximum temperature of the hotspots are proposed that exploit external positivity of the system dynamics (Section IV).

Together, these results provide a framework to understand the formation of thermal hotspots in lithium-ion batteries. They also highlight the value of exploiting positivity properties of lithium-ion battery models to ensure performance bounds are scalable, tight, and able to generalise to arbitrary use profiles.

II. Modelling temperature distributions in lithium-ion battery pouch cells

This section contains two mathematical models of lithium-ion pouch cells that are considered in this work. Section II-A contains the more complex model from [8] that describes distributions of current, state-of-charge, voltage and temperature across the plane of the pouch cell, whilst Section II-C contains a simpler model for the temperature distribution which assumes a constant current distribution across the pouch cell. The code used to produce these results can be found here: `https://github.com/r-drummond/hotspots_control`. Schematics of the models are shown in Figure 1d. Figure 1a has an example of a pouch cell. Figure 1b is a schematic for the model of [8] with equivalent circuit dynamics at each point in the plane whilst Figure 1c is a schematic for (4) with current sources (defined by Assumption 1) distributed. Figure 1d details the 2D domain and boundary conditions for the model of (4).

A. Pouch cell model with current distributions

The pouch cell model from [8], which was used there to optimise graded electrode designs, is recapped. This model is described by a set of partial differential algebraic equations in 2D and is used here as a comparison for the simpler model of Section II-C. The model describes the distribution of current, state-of-charge, and temperature across the plane of the pouch cell, using an equivalent circuit model for the electrical dynamics. The model's variables are given in Table I and its parameters in Table II. These variables are defined in the (y,z)-plane and the dependency of the variables is not shown in the model equations (1) to ease readability.

Defining $\Delta f = \frac{\partial^2 f}{\partial y^2} + \frac{\partial^2 f}{\partial z^2}$ for the 2D diffusion operator, then, following [8], the model equations are described in the domain $\Omega = [0,\, L_y] \times [0,\, L_z]$ by

$$i_x = \frac{V - U(\text{SoC,T}) - v_1 - v_2}{R A_{\text{cell}}}, \tag{1a}$$

$$\Delta V = \frac{i_x}{\bar{\sigma}}, \quad \text{on} \quad \Omega,\ t > 0, \tag{1b}$$

$$\rho \frac{\partial T}{\partial t} = \lambda_{\text{eff}}\, \Delta T + \frac{R\, A_{\text{cell}}\, {i_x}^2 - h_{\text{faces}}\,(T - T_{\text{ref}})}{L_x\ n_{\text{layers}}}, \tag{1c}$$

$$\frac{\partial \text{SoC}}{\partial t} = \frac{A_{\text{cell}}}{C_{\text{cell}}} i_x, \tag{1d}$$

$$\frac{\partial v_1}{\partial t} = -\frac{v_1}{R_1 C_1} + \frac{A_{\text{cell}}}{C_1} i_x, \tag{1e}$$

$$\frac{\partial v_2}{\partial t} = -\frac{v_2}{R_2 C_2} + \frac{A_{\text{cell}}}{C_2} i_x. \tag{1f}$$

Eqn. (1a) is obtained by assuming circuit models [9] are distributed across the plane of the pouch cell as in [8]. Eqn. (1a) defines the through-thickness current density (as in the current density flowing across the electrodes charging the active material particles). Eqn. (1b) is adapted from Taheri *et al.*, [10] to account for the circuit dynamics and defines the distribution of the voltage in the (y,z) plane, given the current density i_x through the cell at each point. Eqn. (1c) defines the localised temperature dynamics of the cell and is adapted from Lin *et al.*, [3] with Joule heating from from Eqn. (1a) replacing that from [3] involving electrochemical potentials. Using the circuit model of [8] for the electrical dynamics at each point (y,z) in the plane (with the derivations of these dynamics discussed in Plett [9]), Eqn. (1d) describes the state-of-charge and Eqns. (1e) - (1f) are the relaxation dynamics of the RC pairs in Figure 1b.

B. Boundary Conditions

Defining $n_\perp$ as the two-dimensional unitary vector normal to the boundary and $\nabla T(y,z,t) = [\partial T/\partial y, \partial T/\partial z]^\top$, the model's boundary conditions can be described by

$$n_\perp \cdot \nabla T = -\frac{h}{\lambda_{\text{eff}}}\,(T - T_{\text{ref}}), \quad \text{on} \quad \partial\Omega_{\text{ext}},\ t > 0, \tag{2a}$$

$$n_\perp \cdot \nabla T = -\frac{h_{\text{tab}}}{\lambda_{\text{eff}}}\,(T - T_{\text{ref}}), \quad \text{on} \quad \partial\Omega_{\text{tab}},\ t > 0, \tag{2b}$$

$$\frac{\partial V}{\partial z}\Big|_{z=L_z} = \frac{I_{\text{app}}}{\sigma_{\text{ck}} A_{\text{tab}}}, \quad \text{on} \quad \partial\Omega_{\text{tab,k}}, k \in \{n, p\}, t > 0, \tag{2c}$$

$$n_\perp \cdot \nabla V = 0, \quad \text{on} \quad \partial\Omega_{\text{ext}},\ t > 0, \tag{2d}$$

with $\partial\Omega_{\text{tab,n}}$ and $\partial\Omega_{\text{tab,p}}$ being the negative and positive tabs, $\partial\Omega_{\text{tab}} = \partial\Omega_{\text{tab,n}} \cup \partial\Omega_{\text{tab,p}}$, $\partial\Omega_{\text{ext}} = \partial\Omega \setminus \partial\Omega_{\text{tab}}$ the external boundary and $\partial\Omega_{\text{ext}}$ the external boundary without the tabs.

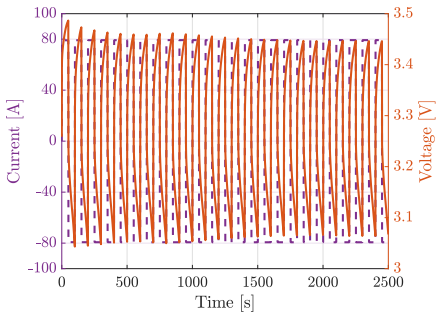

(a) Current and voltage signals during the 4C cycling experiments of Lin et al., [3].

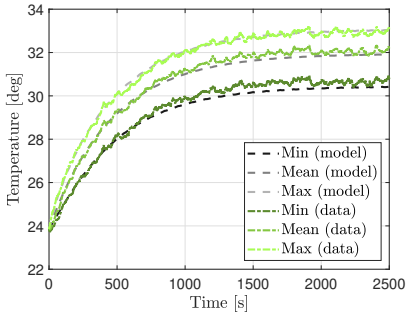

(b) Simulation results of Eqn. (1).

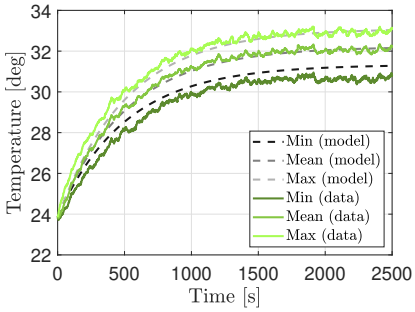

(c) Simulation results of Eqn. (4).

Fig. 2: Maximum, minimum, and average temperatures across the pouch cells. Comparison between the experimental data of [3] with (a) the model from [8] and (b) from (4).

C. Simplified pouch cell model

A simpler model to that of Eqns. (1) and (2) from [8] for the temperature distribution across the pouch cell is now developed. The following assumption will be used for this model simplification.

Assumption 1: As illustrated in Figure 1c, current is distributed evenly across the (y,z)-plane of the pouch cell by

$$i_x \approx \frac{I_{\text{app}}}{A_{\text{cell}}}. \tag{3}$$

Previous modelling studies, including [3], [8], [10], have highlighted the limitation of Assumption 1. In particular, Taheri *et al.*, [10] showed that the current should decrease away from the tabs at a rate proportional to $\cosh(\beta y)$ for some β. These current distributions imply that regions of the pouch cell will react at different rates. For example, during charging, the regions near the tabs will charge first, until they reach their maximum intercalation limits, then the region experiencing the fastest charging rates will propagate down the length of the cell, as discussed in [8].

However, the results of [8], [10] suggest that when the pouch cells are sufficiently small or the current collectors are sufficiently conductive, then Assumption 1 is often satisfactory. Moreover, the benefits of Assumption 1 are that it greatly simplifies the thermal model dynamics. Specifically, (1) simplifies to the single equation

$$\rho \frac{\partial T}{\partial t} = \lambda_{\text{eff}} \Delta T + \frac{R\, A_{\text{cell}} \left(\frac{I_{\text{app}}}{A_{\text{cell}}}\right)^2 - h_{\text{faces}} (T - T_{\text{ref}})}{L_x \; n_{\text{layers}}}, \tag{4}$$

with boundary conditions given by (2a) and (2b). In other words, the partial differential algebraic equations of (1) simplify to the single partial differential equation (4). Through Assumption 1, there is no need to resolve the algebraic equations for the current distribution driving the Joule heating in the pouch cell; instead the distribution is assumed to be flat as the current collectors are sufficiently conductive. The thermal model dynamics of (4) then become simple enough to solve control problems, including computing the temperature hot spot bounds of Section IV which is the main focus presently.

D. Comments

The pouch cell model (4) is a simplification of the model from [8] which is itself a simplification of the model from [3]. Specifically, compared to [8], (4) assumes that the current density distribution is uniform across the plane of the pouch cell (Assumption 1) and, compared to [3], no electrochemical modelling is used to characterise the heat generation. In both [8] and [3], the models are described by differential algebraic equations whose analysis (in terms of the bounds of Section IV) is beyond the scope of this paper. Instead, here, a simpler model is proposed, validated against experimental data, and analysed.

E. Numerical implementation

The PDE model (4) is discretised in space along a $(N+2)\times(N+2)$ grid using spectral collocation following [11]. This spatial grid is defined by the points $(\mathbf{y},\mathbf{z}) \in \mathbb{R}^{N+2} \times \mathbb{R}^{N+2}$. Using spectral collocation for spatial discretisation is a commonly used and robust scheme when modelling electrochemical energy storage devices (e.g., [12] and [13]) as it can accelerate computational times for a given level of solution accuracy.

After applying spectral collocation to (4), a state-space model for the temperature dynamics is obtained. The state of this model is $\mathbf{T}(t) \in \mathbb{R}^{n=N^2}$ which is the spatially discretised relative increase in pouch cell temperature, as in

$$\mathbf{T}_k(t) = T(\mathbf{x}_i, \mathbf{y}_j, t) - T_{\text{ref}},$$

for all $i, j = 2, 3, \ldots, N+1$, and $k = 1, 2, \ldots, N^2 = n$. The discretised thermal model of Eqn. (4) is then

$$\frac{d\mathbf{T}(t)}{dt} = A\mathbf{T}(t) + Bu(t), \tag{5a}$$

$$\mathbf{T}_i(t) = C_i\mathbf{T}(t), \tag{5b}$$

where $\mathbf{T}_i$ is the i^{th} element of the temperature vector $\mathbf{T} \in \mathbb{R}^n$ and $u(t) = I_{\text{app}}(t)^2$. Finally, the transfer function of (5) is

$$G_i(s) = C_i(sI_n - A)^{-1}B, \tag{6}$$

where C_i is the i^{th} standard basis vector.

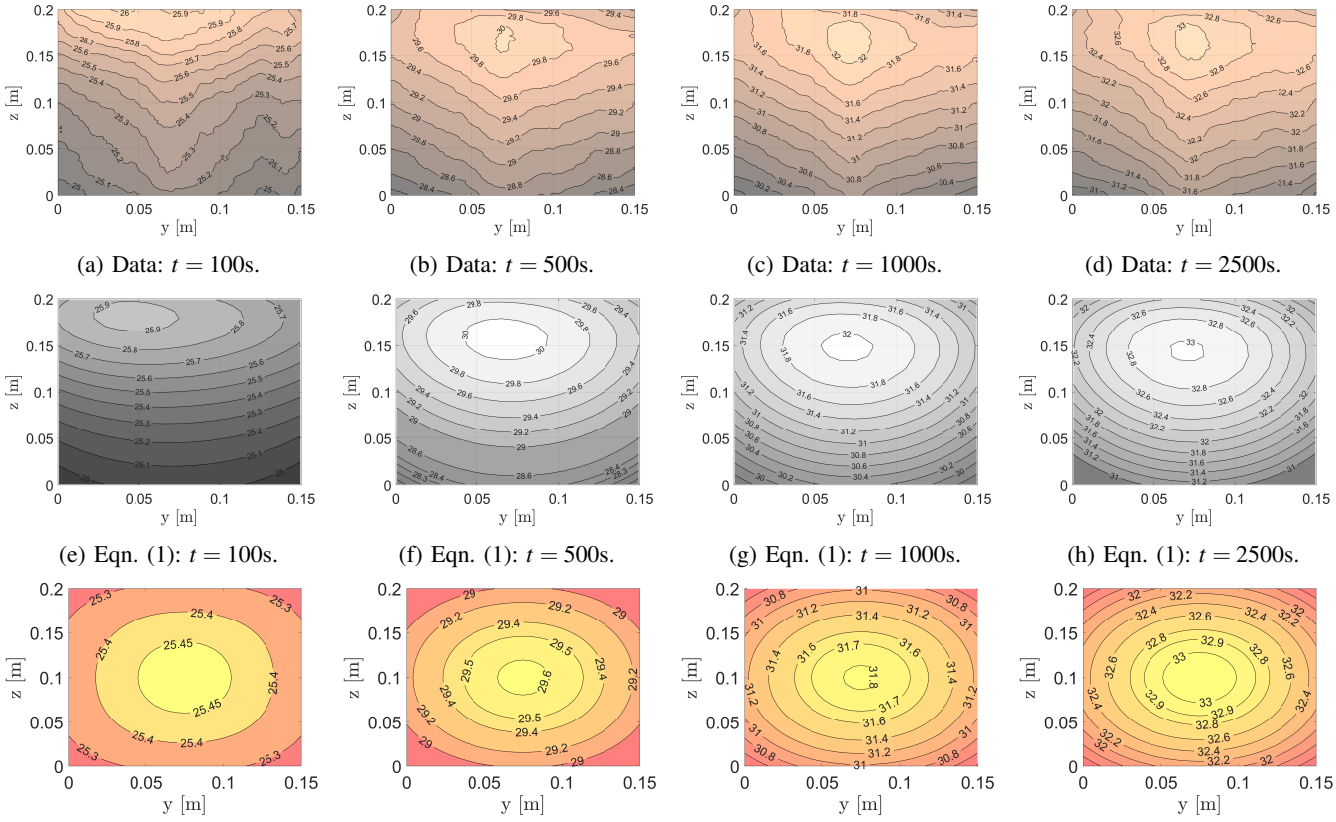

(a) Data: $t = 100$s. (b) Data: $t = 500$s. (c) Data: $t = 1000$s. (d) Data: $t = 2500$s.

(e) Eqn. (1): $t = 100$s. (f) Eqn. (1): $t = 500$s. (g) Eqn. (1): $t = 1000$s. (h) Eqn. (1): $t = 2500$s.

(i) Eqn. (4): $t = 100$s. (j) Eqn. (4): $t = 500$s. (k) Eqn. (4): $t = 1000$s. (l) Eqn. (4): $t = 2500$s.

Fig. 3: Comparison between the experimental data of [3] and the model simulations of (1) and (4). The results are for 4C cycling of a 20 Ah pouch cell from A123 Systems with $LiFePO_4$ positive electrodes and a graphite negative electrodes as detailed in [3]. The comparisons are at snapshots at t = 100s, 500s, 1000s and 2500s during the cycling.

III. Experimental validation

Experimental data from [3] are used to verify the predicted temperature distributions across large format pouch cells from [8] and the simplified model (4). Figures 3 and 4 compare the model's simulations against temperature distribution data from [3] of a 20 Ah pouch cell from A123 Systems with $LiFePO_4$ positive electrodes and a graphite negative electrodes cycled at 4C for 50s. Figure 2a details the current and voltage profiles during these cycling experiments, with the thermal responses shown in Figures 2b, 2c and 3. Even though the model of (4) is relatively simple (compared to both [8] and [3]), Figure 3 shows it is able to capture the main features of the temperature distribution data across the plane of the pouch cell. Figure 3 shows a thermal hot spot forming in the centre of the modelled cell, although this hot spot was located further down the plane compared to the data of [3]. The reason for the drift in the hot spot's position with (4) was due to Assumption 1, as it does not account for the increased current density at the tabs identified in [8] during the start of a cycle. Further validation of the model can be found in Figure 4 which shows close agreement between the minimum, maximum and average temperatures of the experimental data and the two models.

IV. Bounding the temperature distributions across the pouch cell

As seen in the previous section, the experimental data of [3] show the formation of thermal hotspots in pouch cells, which could then influence both their ageing and electrochemical response [3]. The aim of this section is to bound these hotspots. In other words, the goal is to provide certificates for the maximum temperature reached by the pouch cell during some arbitrary use profile.

Two methods are proposed to bound the hotspots. The first, solves a semi-definite programme whereas the second exploits the external positivity of the thermal dynamics to bound them using the system's DC gain. In this way, the results highlight the potential of exploiting positivity of the system dynamics to simplify analysis and control problems for lithium-ion batteries.

A. Semi-definite programming approach

The first approach to bound the temperature distribution across the pouch cell is based on the peak-to-peak gains of [14]. The following proposition gives an upper bound of the output, that is $\sup_{t\geq 0}\|T_i(t)\| =: \|T_i\|_\infty$, given an upper bound on the input, that is $\sup_{t\geq 0}\|u(t)\| =: \|u\|_\infty$; it is, in principle, tractable but not tight.

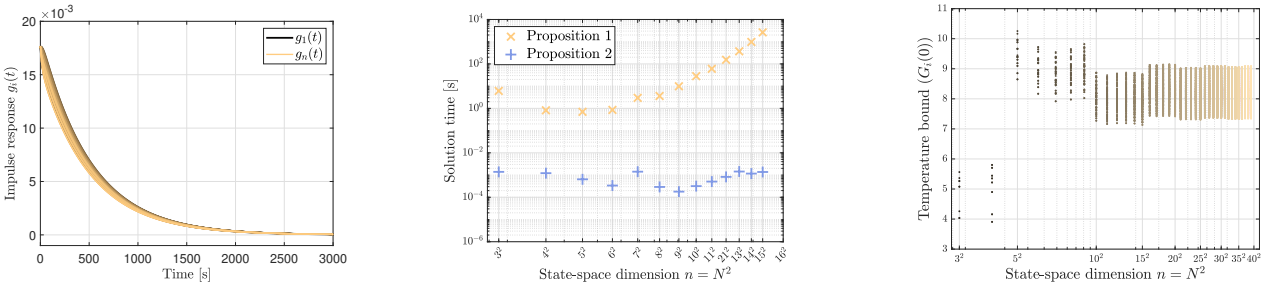

(a) Impulse responses $g_i(t)$ of the pouch cell model (5) with $N = 24$.

(b) Compute times for Propositions 1 and 2 as functions of the discretisation elements N.

(c) The bounds of Proposition 2 as the number of discretisation elements N increases.

Fig. 4: Comparison between the bounds of Propositions 1 and 2. (a) verifies that the linear systems $G_i(s)$ are externally positive and so Assumption 2 is satisfied. (b) compares the computation times of the two bounds. (c) shows the evolution of the bound of Proposition 2 as the number of discretisation elements, N, increases.

Proposition 1: If there exists $P \succ 0$, $\lambda \geq 0$, $\zeta \geq 0$ and

$$\min \quad \zeta \tag{7a}$$

$$\text{subject to} \quad \begin{bmatrix} A^\top P + PA + \lambda P & PB \\ (PB)^\top & -\zeta \end{bmatrix} \prec 0, \tag{7b}$$

$$\begin{bmatrix} \lambda P & C_i{}^\top \\ C_i & \zeta \end{bmatrix} \succeq 0, \ \forall i = 1, 2, \ldots, n, \tag{7c}$$

then $\|\mathbf{T}_i\|_\infty \leq \zeta \|u\|_\infty$ for all $u \in \mathscr{L}_\infty$ from $\mathbf{T}(0) = 0$.

Proof: Follows from [14]. ∎

Evaluating Proposition 1 requires the solution of a generalised eigenvalue problem (GEVP) or a semi-definite program (SDP) with a line search due to the bilinearity arising from the product λP. Therefore, Eqn. (7) scales poorly as the dimension of the system (as in the number of discretisation nodes N of (5)) increases. Even though spectral collocation discretisation can help to reduce the number of discretisation nodes needed for an accurate solution, the dimension of the state-space of (5) can still be large. For example, the simulations of Figure 3 required $N = 24$ and so $n = 24^2 = 576$ states. This number is still significantly smaller than the state-space of the more complex model of (1) which has six spatially distributed variables changing in time, as in $i_x, V, T, \text{SoC}, v_1$, and v_2, and so the resulting discretised would have $6N^2$ variables. Moreover, these model dynamics contain both differential and algebraic equations which can be more challenging to analyse and simulate. Thus, whilst Proposition 1 is arguably the "*standard*" control approach for bounding system responses (as evidenced by the widespread use of [14]), its computational intractability arguably limits its value here for bounding thermal hotspots in pouch cells.

B. Bound based upon the DC gain

To overcome this computational complexity, a more scalable method to bound the maximum increase in temperature of the pouch cell is proposed. The main idea is to exploit *external positivity* of the transfer function from $u(t) = I_{\text{app}}(t)^2$ to $\mathbf{T}_i(t)$ of the model from Eqn. (5).

Definition 1: A transfer function $G_i(s) = C_i(sI_n - A)^{-1}B$ with impulse response $g_i(t)$ is said to be *externally positive* if $g_i(t) \geq 0$ for all $t \geq 0$.

Assumption 2: For each $i = 1, 2, \ldots, n$, the transfer functions $G_i(s)$ of model (5) are externally positive.

Positivity properties of lithium-ion battery models have previously been used to simplify and scale up the analysis of lithium-ion battery algorithms, e.g. for fast charging [15] and designing pack-level battery management systems [16]. More broadly, positive systems theory has been successfully used to provide scalable certificates for many control problems, most notably through the results of Rantzer in [17]. Inspired by these results, the following proposition uses the fact from [17] that the maximum gain of an externally positive transfer function is bounded by its DC gain to bound the rise in temperature across a pouch cell.

Proposition 2: Define $\|{I_{\text{app}}}^2\|_\infty = {I_{\max}}^2$. Imposing Assumption 2 and that the temperature dynamics of the pouch cell are defined by (4), it follows that

$$\mathbf{T}_i(t) \leq G_i(0){I_{\max}}^2 = -C_i A^{-1} B \ {I_{\max}}^2 \quad \forall t \in [0, \infty).$$

Proof: Since $\mathbf{T}_i(t) \geq 0$ for all $t \geq 0$ as a result of Assumption 2 and as $u(t) = I_{\max}^2 \geq 0$, we obtain:

$$\begin{aligned} \mathbf{T}_i(t) &= \int_0^t g_i(t-\alpha) {I_{\text{app}}(\alpha)}^2 \ \mathrm{d}\alpha \\ &\leq {I_{\max}}^2 \int_0^\infty g_i(\alpha) \ \mathrm{d}\alpha = {I_{\max}}^2 \ G_i(0). \end{aligned}$$

∎

Remark 1: If $u(t) = I_{\text{app}}(t)^2$ is constant, then the above inequality is sharp (in the sense that it becomes an equality) in the limit as t gets large. Constant current cycling, such as that considered in [3] and shown here in Figure 3, is an example of such a scenario.

C. Verifying external positivity of the pouch cell model

In order to apply Proposition 2, external positivity of $G_i(s)$ must be verified. Verifying externally positivity is, in general, challenging [17], [18], although in some cases it can be easily checked. For example, diffusion systems, such as those described by (4), are closely related to *relaxation systems* in finite dimensions which are externally positive. However, here, the two dimensional nature of the model, and the use of spectral collocation for the discretisation, complicate the problem of verifying external positivity of

$G_i(s)$. As an alternative, it is proposed to simply verify these positivity properties graphically. This is shown in Figure 4a where the impulse responses $g_i(t)$ for $i = 1, 2, \ldots, n = N^2$ with $N = 24$ are shown. External positivity is clear from the trajectories. Whilst this graphical inspection is not formal, it provides a simple test to verify Assumption 2 for (5), and so enable the use of the more computationally efficient method of Proposition 2 to bound the thermal hot spot.

V. Results

This section evaluates the use of Propositions 1 and 2 to bound the maximum temperatures of the lithium-ion battery pouch cells. The results are shown in Figure 4.

Figure 4b compares the compute times for Propositions 1 and 2 as functions of the number of discretisation elements N^2. The SDPs of Propositions 1 scales rapidly with the grid size N, and could not be evaluated above $N > 17$ due to a lack of RAM. By contrast, Proposition 2 did not suffer from this scaling, as it just required evaluating $G_1(0)$.

Figure 4c evaluates how the bounds of Proposition 2 vary with the number of discretisation elements N. Each dot in the figure corresponds to a value of $G_i(0)$ for $i = 1, 2, \ldots, N^2$ and then sweeps through $N = 3, 4, \ldots, 39$. The figure shows the bounds eventually converging to $\mathbf{T}_1(t) < 9.0759$, a value in agreement with the simulation results of Figure 2c. The tightness of these bounds supports the message of this paper that the model (5) and Proposition 2 could be used to tightly bound the maximum value of the pouch cell's thermal hot spot for arbitrary use profiles.

Conclusions

The paper proposed a method to bound the maximum temperature in a lithium-ion pouch cell. A computationally efficient model for the temperature distribution in the pouch cell was validated against experimental data from Lin *et al.*, [3]. Bounds for the model's maximum temperature using external positivity of the dynamics were proposed and shown to significantly improve computation times. Moreover, for constant current cycling, the obtained bounds are tight. These proposed results could be used to characterise the thermal behaviour of pouch cells and support the development of battery management system algorithms and pack designs.

Parameter	Description	Units	Value
A_{tab}	Area of a tab	m^2	1.56×10^{-4}
A_{cell}	Cell area ($L_y \times L_z$)	m^2	30×10^{-3}
n_{layers}	# of layers in cell		42
C_{cell}	Capacitance (20 Ah)	A s	20 $\times$3600
C_1	Capacitance of RC-pair	F	2.79×10^{4}
C_2	Capacitance of RC-pair	F	8.89×10^{3}
h	Heat transfer coefficient	$\text{W m}^{-2}\ \text{K}^{-1}$	11.0
h_{tab}	Heat transfer coefficient of tabs	$\text{W m}^{-2}\ \text{K}^{-1}$	51.58
h_{faces}	Effective heat transfer coefficient of current collector faces	$\text{W m}^{-2}\ \text{K}^{-1}$	$210\times L_x$
L_{cn}	Thickness of negative current collector in x direction	μm	25
L_{cp}	Thickness of positive current collector in x direction	μm	25
L_{x}	Electrode thickness	m	$110\ \times10^{-6}$
L_{y}	Height of battery	m	0.2
L_{z}	Width of battery	m	0.15
R_0	Series resistance of Uniform cell	Ω	1.5×10^{-3}
R_1	Resistance of RC-pair	Ω	1.10×10^{-3}
R_2	Resistance of RC-pair	Ω	2.25×10^{-4}
T_{ref}	Reference temperature	K	298.15
λ_{eff}	Effective thermal conductivity	$\text{W m}^{-1}\ \text{K}^{-1}$	4.5
ρ	Volumetric heat capacity	$\text{J K}^{-1}\ \text{m}^{-3}$	$1.35\ \times10^{5}$
σ_{cn}	Electronic conductivity of copper negative current collector	S m^{-1}	5.96×10^{7}
σ_{cp}	Electronic conductivity of aluminium positive current collector	S m^{-1}	3.77×10^{7}
$\bar{\sigma}$	Effective conductivity	S	$\frac{L_{\text{cn}}L_{\text{cp}}\ \sigma_{\text{cn}}\ \sigma_{\text{cp}}}{\sigma_{\text{cn}}L_{\text{cn}}+\sigma_{\text{cp}}L_{\text{cp}}}$

TABLE II: Model parameters. Values obtained from [3] and [8] for a 20 Ah capacity cell.

References

[1] J. T. Frith, M. J. Lacey, and U. Ulissi, "A non-academic perspective on the future of lithium-based batteries," *Nature Communications*, vol. 14, no. 1, p. 420, 2023.

[2] N. Kirkaldy, M. A. Samieian, G. J. Offer, M. Marinescu, and Y. Patel, "Lithium-ion battery degradation: Comprehensive cycle ageing data and analysis for commercial 21700 cells," *Journal of Power Sources*, vol. 603, p. 234185, 2024.

[3] J. Lin, H. N. Chu, D. A. Howey, and C. W. Monroe, "Multiscale coupling of surface temperature with solid diffusion in large lithium-ion pouch cells," *Communications Engineering*, vol. 1, no. 1, p. 1, 2022.

[4] S. Puls, E. Nazmutdinova, F. Kalyk, H. M. Woolley, J. F. Thomsen, Z. Cheng, A. Fauchier-Magnan, A. Gautam, M. Gockeln, S.-Y. Ham *et al.*, "Benchmarking the reproducibility of all-solid-state battery cell performance," *Nature Energy*, vol. 9, no. 10, pp. 1310–1320, 2024.

[5] X.-G. Yang, T. Liu, Y. Gao, S. Ge, Y. Leng, D. Wang, and C.-Y. Wang, "Asymmetric temperature modulation for extreme fast charging of lithium-ion batteries," *Joule*, vol. 3, no. 12, pp. 3002–3019, 2019.

[6] H. N. Chu, S. U. Kim, S. K. Rahimian, J. B. Siegel, and C. W. Monroe, "Parameterization of prismatic lithium–iron–phosphate cells through a streamlined thermal/electrochemical model," *Journal of Power Sources*, vol. 453, p. 227787, 2020.

[7] A. Trivella, S. Radrizzani, and M. Corno, "Numerical stability analysis of a distributed thermal model for pouch cell assemblies via Gershgorin Circle Theorem," *IEEE Control Systems Letters*, 2025.

[8] R. Drummond, E. Tredenick, T. L. Kirk, M. Forghani, P. Grant, and S. Duncan, "Graded lithium-ion battery pouch cells to homogenise current distributions and reduce lithium plating," *Journal of The Electrochemical Society*, 2025.

[9] G. L. Plett, *Battery management systems, Volume II: Equivalent-circuit methods*. Artech House, 2015.

[10] P. Taheri, A. Mansouri, M. Yazdanpour, and M. Bahrami, "Theoretical analysis of potential and current distributions in planar electrodes of lithium-ion batteries," *Electrochimica Acta*, vol. 133, pp. 197–208, 2014.

[11] L. N. Trefethen, *Spectral methods in MATLAB*. SIAM, 2000.

[12] A. M. Bizeray, S. Zhao, S. R. Duncan, and D. A. Howey, "Lithium-ion battery thermal-electrochemical model-based state estimation using orthogonal collocation and a modified extended Kalman filter," *Journal of Power Sources*, vol. 296, pp. 400–412, 2015.

[13] R. Drummond, D. A. Howey, and S. R. Duncan, "Low-order mathematical modelling of electric double layer supercapacitors using spectral methods," *Journal of Power Sources*, vol. 277, pp. 317–328, 2015.

[14] C. Scherer, P. Gahinet, and M. Chilali, "Multiobjective output-feedback control via LMI optimization," *IEEE Transactions on automatic control*, vol. 42, no. 7, pp. 896–911, 1997.

[15] R. Drummond, N. E. Courtier, D. A. Howey, L. D. Couto, and C. Guiver, "Constrained optimal control of monotone systems with applications to battery fast-charging," *arXiv preprint arXiv:2301.07461*, 2023.

[16] D. Zhang, L. D. Couto, P. Gill, S. Benjamin, W. Zeng, and S. J. Moura, "Interval observer for SOC estimation in parallel-connected lithium-ion batteries," in *Procs. of the American Control Conference (ACC)*. IEEE, 2020, pp. 1149–1154.

[17] A. Rantzer, "Scalable control of positive systems," *European Journal of Control*, vol. 24, pp. 72–80, 2015.

[18] L. H. Taghavian, "Externally positive systems: Analysis and control based on combinatorial polynomials," Ph.D. dissertation, KTH Royal Institute of Technology, 2024.